Rectification, Gating Voltage, and Interchannel Communication of Nanoslot Arrays due to Asymmetric Entrance Space Charge Polarization

Gilad Yossifon, Yu-Chen Chang, and Hsueh-Chia Chang*

Department of Chemical and Biomolecular Engineering, Center for Microfluidics and Medical Diagnostics, University of Notre Dame, Notre Dame, Indiana 46556, USA

(Received 20 November 2008; published 8 October 2009)

A nanoslot array with a uniform surface charge and height but with asymmetric slot entrances is shown to exhibit strong rectification, gating type current-voltage characteristics and a total current higher than the sum of isolated slots at a large voltage. Unlike previous reports of low-voltage current rectification within nanopores and nanochannels with a nonuniform surface charge and/or height, the asymmetry is due to asymmetric space-charge polarization and interslot communication at only one of the two different entrances.

DOI: 10.1103/PhysRevLett.103.154502 PACS numbers: 47.61.Fg, 47.20.Ma, 47.57.jd, 82.39.Wj

In recent years, the fabrication of nanochannels with overlapping double layers has produced simple single-pore chip models of ion-selective nanoporous membranes for desalination and dialysis or biological ion channels on cell membranes. As a result, the nonlinear ion transport (due to selective filtering of cations or anions at the entrance by ion-selectivity endowed by overlapping double layers) [1] and the resulting ion enrichment or depletion [2], overlimiting current [3] and ionic current rectification [4–6] phenomena, can be examined to reveal the mechanisms behind many curious nonlinear *I–V* behavior of ion-selective membranes. This effort could lead to ionic equivalents of electronic circuits, such as triodes and transistors, to tailor design smart membranes for desalination, molecular sieving, artificial cells, etc.

An important and yet relatively unexplored *I–V* characteristic of conducting ion-selective membranes and fabricated nanochannels of Fig. 1 is that, at sufficiently high voltages, its current density often exceeds the limiting current density predicted by the classical diffusion-limited current transport theory [7]. Below the critical voltage for this overlimiting current, the *I–V* curve assumes initially a linear Ohmic relationship that with further increase of the voltage saturates to an almost constant limiting current density level. As shown in the numerical simulation results in Fig. 2 for the particular device in Fig. 1, an electroneutral diffusion layer (DL) with a large ion concentration gradient [Fig. 2(a)] appears next to the influx entrance of the nanoslot (a nanochannel whose width $\gg$ height/depth, wherein the width is in the y direction, and the height is normal to the x-y plane) or one surface of a nanoporous membrane, where counterions enter the nanoslot, to enhance the flux via diffusion. When the ion concentration at the nanoslot surface approaches zero and the concentration drop across the DL cannot increase further, the current density approaches a limiting value as predicted by Levich [7]. Later theories by Rubinstein and Shtilman [8] suggest that, at higher voltages, an extended polarized layer (EPL, or equivalently, space-charge layer—SCL), much thicker than the electric Debye layer (EDL) thickness λ, can appear between the EDL and the DL to sustain the overlimiting current density, which can be significantly higher than the limiting current density, with a lower differential resistance than the Ohmic value {Fig. 3(a), in agreement with [3]}. These three different layers are collectively termed the concentration polarization layer [CPL, Fig. 2(c)]. As ion electromigration in a region with space charge is a nonlinear phenomenon, nonlinear *I–V* characteristics develop at high voltages with a differential resistance determined by the dimension L of the CPL layer on the influx interface.

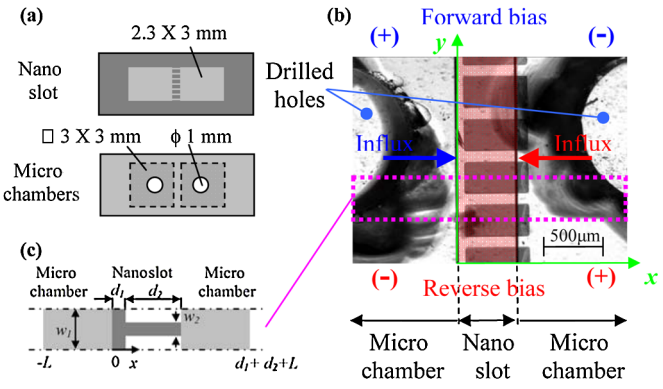

FIG. 1 (color online). An intentional misalignment of the two Pyrex slides (a) results in asymmetric nanoslot entrances to the microchambers, as seen in the optical microscope image (b) (top view—normal to the uniform nanoslot depth $h = 190$ nm). On the right side, the separate nanoslots exit directly into the microchamber, while on the left side, they first merge into a wide slot which in turn exits into the microchamber. The influx direction associated with the different voltage biases represents the flow direction of the counterions into the nanoslot. The geometric parameters of the slot are $d_1 = 50$ μm, $d_2 = 450$ μm, $w_1 = 350$ μm, $w_2 = 100$ μm, based on the simplified theoretical model depicted in (c) (top view) which represents one cell of a periodic array (in the y-direction) of the actual asymmetric (in the x direction) nanoslot array (b).

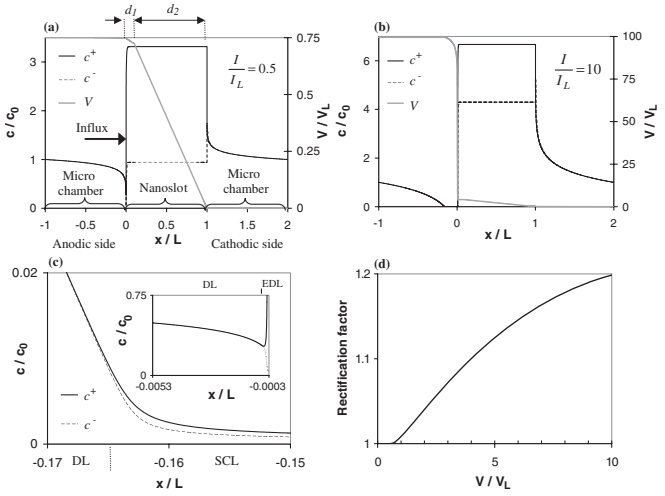

FIG. 2. Numerical computation results for the concentration and voltage profiles across the asymmetric periodic cell [Fig. 1(c)] below (a) and beyond (b) the limiting current I_L. The electric resistance clearly shifts from the nanoslot in (a) to a small polarized layer at the left anodic entrance in (b), which is blown up in (c). Note that c^- and c^+ are identical outside the nanoslot (electroneutrality condition) except for the small polarized layer (c). Increase of the rectification factor with the voltage is depicted in part (d) of the figure. Reverse bias profiles are qualitatively similar but of opposite concentration and voltage trends. The normalized values of $\Sigma/c_0 = 2$, $(d_1 + d_2)/L = 1$, $\delta = \lambda/L = 2 \times 10^{-5}$, and $h/L = 3.8 \times 10^{-4}$ have been used.

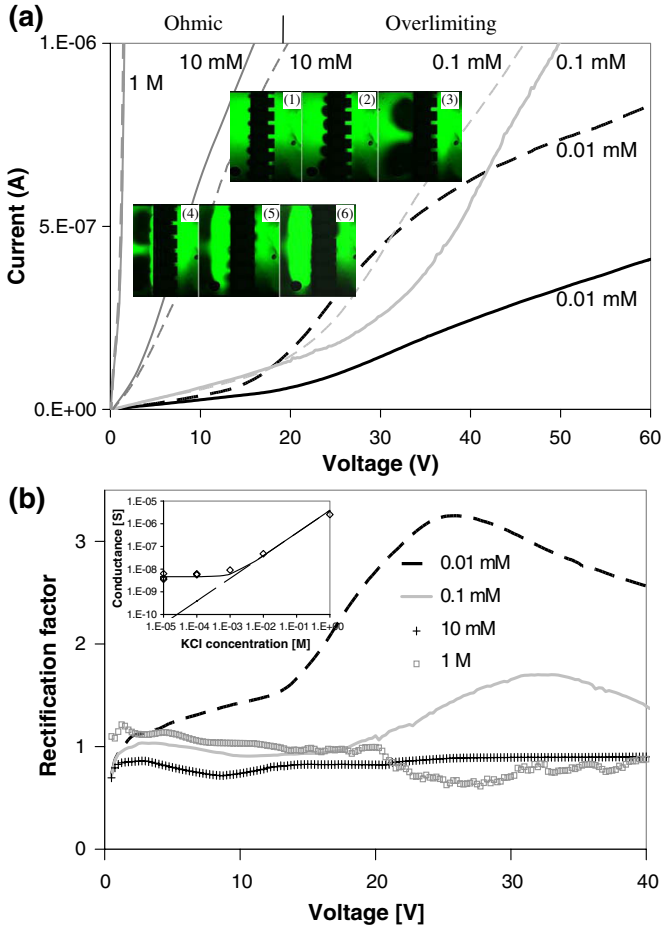

FIG. 3 (color online). (a) I–V measurements of the device in Fig. 1 for varying ionic strengths and applied voltages (continuous lines: reverse bias; dashed lines: forward bias). Upper (1–3) and lower (4–6) insets of part (a) of the figure depict the evolution (at three time instances) of the depletion-enrichment phenomenon under forward and reverse 30 V bias, respectively. In the former, the depletion layer evolves at the left hand side of the nanoslot, while the opposite in the latter. (b) The measured rectification factor versus voltage for the data in part (a) of the figure. Inset depicts the conductance of the nanoslot array as a function of solution concentration [symbols—experiment; continuous line—model (Eq. 13, [13]); dashed line—bulk conductivity {model (Eq. 13, [13]) with $\Sigma = 0$}]. A fitted value of $|\sigma| = 21.7$ mC/m^2 (corresponding to a fixed volume charge density $zF\Sigma = -2\sigma/h$ of about $\sim$229 KC/m^3, wherein z denotes the ion valency and F the Faraday number) was obtained for the surface charge density.

As we verified earlier [9], the mechanism for selecting the CPL thickness L involves an electroconvection instability of the SCL, another nonlinear phenomenon, at the influx side [10]. The onset of the instability is controlled by an over voltage [10], as is evident from the measured I–V curve in Fig. 3(a), wherein the overlimiting region associated with this instability appears only beyond a critical voltage ($\sim$15–20 V). This vortex instability develops into a stationary vortex array [insets 1–3 of Fig. 3(a)] on the interface with a steady thickness that determines the CPL. How the electroconvection instability selects L remains unknown, but its onset is clearly controlled by the applied voltage, the ion selectivity and the nanoslot depth [9].

Previous studies of ionic current rectification through nanopores or nanochannels [4–6], which is similar to that found in biological ion channels [11], have all been restricted to relatively small voltages (i.e., Ohmic region). Rectification factor for these nanopores is defined as a ratio of currents recorded for voltages of the same amplitude but opposite polarities and are attributed to a mechanism analogous to that of a semiconductor bipolar diode [12]. Instead of asymmetric doping across a p-n junction to produce a potential barrier, an *interior* asymmetry of the equilibrium (i.e., prior to applying an external electric field) electrochemical potential is introduced to produce a potential well that detains the counterions from passing freely through the nanopore. The nonuniform equilibrium electrochemical potential distribution is obtained via geometric variations so as to control the EDLs overlap intensity [4], surface charge patterning [5], and a combination of these two [6].

A minute voltage drop across the extremely thin membrane like a biological cell wall may result in electric fields that exceed the Ohmic region. In the current study, we tested a new asymmetric (in the x direction) nanoslot device (Fig. 1) whose rectification occurs only in the overlimiting region beyond a certain gating voltage. In contrast to previous studies of diodelike nanofluidic devices, our nanoslot is of uniform height/depth h and surface charge σ

(i.e., uniform *equilibrium* electrochemical potential), hence, no rectification is expected to occur in the Ohmic region. As shown in Fig. 1, the nanoslot is bounded by two square-shaped microchambers with much larger depths. As the SCL and its electroconvection instability appear only at the influx entrance of the nanoslot [Figs. 2(b) and 2(c)] and as both control the overall current flux [most of the voltage drop occurs across the SCL, in contrast to the Ohmic case wherein it falls across the nanochannel—compare Figs. 2(a) and 2(b)], the asymmetric entrances on two sides of the periodic (in the y direction) nanoslot array (Fig. 1) can produce different SCLs and generate a rectification phenomenon. On the right side in Fig. 1(b), each of the nanoslots in the array drains directly into the deep microchamber, while on the opposite side, they first merge into another slot with the same width as the microchamber but the same height as the nanoslot, before it in turn drains into the other microchamber.

The theoretical model used is based on that derived in [13] for a nanoslot geometry wherein radial field focusing effect is taken into account, and extended to the nanoslot array by considering the single nanoslot periodic cell [Fig. 1(c)] with periodic boundary conditions in the y direction. The change of the slot width from w_1 to w_2 over a slot length of d_1 at the left entrance [Fig. 1(c)], representing the wide nanoslot that connects the narrower one to the left microchamber, is accounted for by appropriate matching conditions of the electric field and ionic flux continuity (i.e., the one-dimensional flux within the narrower nanoslot section is a factor of w_1/w_2 higher than that in the wider nanoslot section). The degree of boundary asymmetry is measured by $d_1/(d_1 + d_2)$, but its precise value is unimportant so long as it is not too small (i.e., an array of narrow separated nanoslots of width w_1) or close to 1 (i.e., a single wide nanoslot), since the SCL region does not penetrate much into the nanoslot. Similar to Manazanares *et al.* [14], the nanoslot surface charge is replaced by an effective volumetric concentration Σ to produce an effective one-dimensional (in the x-direction) homogenized model that has been averaged over both the nanoslot height and width. Using such a model, the distinct ion distributions and *I–V* characteristics in the Ohmic and overlimiting current regimes are numerically computed from the ion transport equations and the Poisson equation, and are shown on both sides of the nanoslot array in Fig. 2. Note that the CPL on the anodic influx side controls the *I–V* characteristics and exhibits all the signature ion distributions in the various regimes. The enrichment side on the cathodic side is always electroneutral (outside a thin equilibrium EDL) without a polarized layer.

The chip containing the nanoslot array was fabricated using standard photolithography technologies [15] and consists of seven nanochannels connected between two microchambers of ~ 28 μm in depth (see [16] for further chip fabrication details). Reservoirs made of flexible silicone were used on top of the holes wherein platinum electrodes ($\phi 0.3$ mm) were introduced. Different dilutions of 1 M potassium chloride (KCl) were used (see [16] for more details) to change the ionic strength and control the degree of EDL overlap.

To obtain the measured *I–V* curves in Fig. 3, the applied voltage was stepped in 0.25 V increments every 3 s, during which time current transients were observed to decay completely. Using bipolar diode terminology, the reverse bias is defined when the anode is on the right side of the nanoslot [without an intermediate nanoslot; Fig. 1(b)], and the opposite for the forward bias. In the low concentration limit, a linear Ohmic region followed by an overlimiting one is clearly seen [Fig. 3(a)], with the transition point ($\sim$15 V) approximating Levich's limiting current density. Note that only the Ohmic and overlimiting regions are indicated in the *I–V* curve, whereas the intermediate limiting current region [13] is omitted due to its negligible length. These data are in qualitative agreement with previous experimentally obtained *I–V* curves for true nanoporous membranes ([17]) and also for nanochannels [3,11,13]. Interestingly, the electrical conductance in the overlimiting region is significantly higher than that in the Ohmic region (in agreement with [3]), resulting in a voltage gating like *I–V* characteristics reminiscent of cell membrane ion channels [18]. It is associated with the instability selecting a much smaller CPL length than the distance between the nanoslot entrance to the electrode [13], hence, increasing the diffusion limited current. At high enough concentrations ($>10^{-3}$ M), only the Ohmic region is observed as the thinner Debye length stipulates that EDLs overlap within the slot and the associated ion perm selectivity is lost [inset of Fig. 3(b)].

As shown in Fig. 3(b), the rectification effect increases with EDLs overlap intensity. For high enough concentrations ($>10^{-3}$ M), there is no rectification (i.e., a rectification factor, defined as the ratio of the forward to reverse bias current, of unity) and gating voltage effects. For the lowest concentration tested of 10^{-5} M, the rectification factor reaches a maximum value ($\sim$3.2) close to the ratio between the entrance's cross sections (i.e., $w_1/w_2 = 3.5$). It is also seen that this rectification occurs beyond the gating voltage (i.e., Ohmic to overlimiting transition) in accordance with Fig. 3(a). The rectification factor in the Ohmic region is negligible, while beyond the gating voltage, it increases with the voltage until reaching a maximum value from which it slowly decays. This is in agreement with the theoretical model [Fig. 2(d)], except the decaying part which is not captured by the model. This suggests that a deviation from the model assumption of *unbounded* radial focusing of the microchamber field lines into the nanoslot occurs. As the selected CPL thickness increases with the voltage [9], both the presence of lateral (y direction) finite dimensions of the device and the microchamber ceiling may come into effect.

The insets of Fig. 3(a) depict the evolution of the depletion-enrichment layers under 30 V of different voltage bias as obtained by confocal microscopy (the event can be observed in the videos [16]), using a buffer and fluorescent

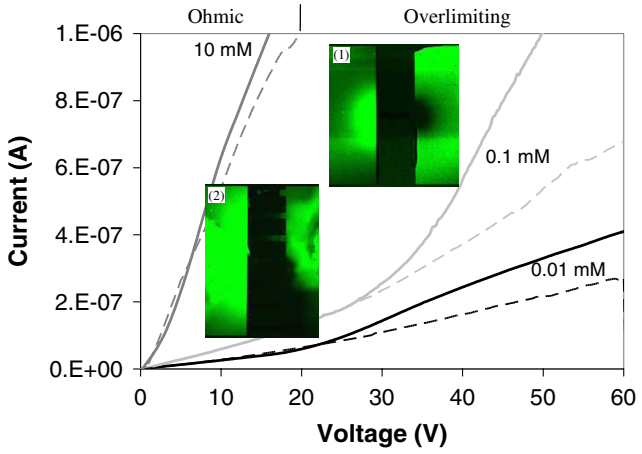

FIG. 4 (color online). Comparison of I–V measurements under reverse bias of the seven-nanoslot array (solid line) versus seven times the current measured across an isolated single nanoslot device (dotted line). The upper (1) and lower (2) insets depict the depletion-enrichment phenomenon under reverse 40 V bias for a single versus a nanoslot periodic array, respectively.

dye molecules (Rhodamine) concentrations of about 10^{-5} M. Under forward bias (insets 1–3) and beyond the gating voltage, the vortex instability originates along the entire slot entrance in the form of a vortex pairs pattern. A complex process of vortex pair wavelength selection takes place through fusion and merging of the vortex pairs into still larger vortex pairs ([8,9]). In contrast, under reverse bias (insets 4–6), a single vortex pair is associated with each of the narrower nanoslots at early stages. Once the depletion layers of the individual nanoslots grow to a sufficient thickness, they start to overlap, and a complex process of vortex pair wavelength selection takes place, similarly to that occurring in the opposite wide slot entrance. Hence, the current through spatially synchronized channels is not equal to the sum of the same through independent nanoslots. Asymmetric entrance conditions have produced different SCL interaction between neighboring nanochannels to produce very different net currents.

That internanoslot interaction across entrance SCL in the overlimiting region can profoundly affect the net ion flux is more conclusively verified with single-channel and multichannel I–V measurements in Fig. 4. In contrast to the Ohmic region, the array current is significantly higher than the corresponding multiple of the single-slot current in the overlimiting region. The overlapping of the depletion and enrichment regions of adjacent nanoslots is clearly evident in the insets of Fig. 4 (the event can be observed in the videos [16]) when the current enhancement due to channel interaction is observed at reverse 40 V bias.

As rectification and current-enhancing channel interaction in the overlimiting region are both sensitively dependent on the micro-nano transverse (y direction) dimension ratio w_1/w_2, they can both be dramatically enhanced by controlling the pore/channel separations. Interestingly, the polarized SCL rectification mechanism at high voltages acts oppositely from that previously reported in nanopores with Ohmic rectification characteristics at low voltages [4–6]. For a homogenous negatively charged conical nanopore, the forward bias (higher current) occurs when the anode is on the tip side of the cone, while rectification in the overlimiting region is exactly the opposite. Together with the high current at the overlimiting region beyond the gating voltage, judicious application of rectification and controlled synchronization between isolated nanochannels/pores may lead to the realization of smart, high-throughput nanoporous membranes for selective ion and molecular sieving.

We are grateful to Profs Y. Zhu and A. Seabaugh for the use of their equipment and for their advice and for the help of P. Mushenheim in conducting the experiments.

*Corresponding author: hchang@nd.edu

[1] D. Stein, M. Kruithof, and C. Dekker, Phys. Rev. Lett. **93**, 035901 (2004).
[2] Q. Pu, J. Yun, H. Temkin, and S. Liu, Nano Lett. **4**, 1099 (2004); A. Plecis, R. B. Schoch, and P. Renaud, Nano Lett. **5**, 1147 (2005).
[3] S. J. Kim *et al.*, Phys. Rev. Lett. **99**, 044501 (2007).
[4] C. Wei, A. J. Bard, and S. W. Feldberg, Anal. Chem. **69**, 4627 (1997); Z. Siwy and A. Fulinski, Phys. Rev. Lett. **89**, 198103 (2002); J. Cervera, B. Schiedt, and P. Ramirez, Europhys. Lett. **71**, 35 (2005).
[5] P. Chen, T. Mitsui, D. B. Farmer, J. Golovchenko, R. G. Gordon, and D. Branton, Nano Lett. **4**, 1333 (2004); Z. Siwy, E. Heins, C. C. Harrell, P. Kohli, and C. R. Martin, J. Am. Chem. Soc. **126**,10850 (2004); Karnik *et al.*, Nano Lett. **7**, 547 (2007).
[6] I. Vlassiouk and Z. S. Siwy, Nano Lett. **7**, 552 (2007).
[7] V. G. Levich, *Physicochemical Hydrodynamics* (Prentice-Hall, New York, 1962).
[8] I. Rubinstein and L. Shtilman, J. Chem. Soc., Faraday Trans. 2 **75**, 231 (1979); I. Rubinstein and B. Zaltzman, Phys. Rev. E **62**, 2238 (2000).
[9] G. Yossifon and H.-C. Chang, Phys. Rev. Lett. **101**, 254501 (2008).
[10] I. Rubinstein, E. Staude, and O. Kedem, Desalination **69**, 101 (1988).
[11] Jiang *et al.*, Nature (London) **417**, 523 (2002).
[12] S. M. Sze, *Modern Semiconductor Device Physics* (Wiley Interscience, New York, 1998).
[13] G. Yossifon, P. Mushenheim, Y. C. Chang, and H.-C. Chang, Phys. Rev. E **79**, 046305 (2009).
[14] J. A. Manazanares *et al.*, J. Phys. Chem. **97**, 8524 (1993).
[15] V. G. Kutchoukov *et al.*, Sens. Actuators A, Phys. **114**, 521 (2004).
[16] See EPAPS Document No. E-PRLTAO-103-016940 for supplementary materials. For more information on EPAPS, see http://www.aip.org/pubservs/epaps.html.
[17] F. Maletzki, H. -W. Rosler, and E. Staude, J. Membr. Sci. **71**, 105 (1992); I. Rubinshtein *et al.*, Russ. J. Electrochem. **38**, 853 (2002).
[18] J. Keener and J. Sneyd, *Mathematical Physiology* (Springer-Verlag, New York, 1998).